communications physics

Article

https://doi.org/10.1038/s42005-024-01898-x

Hour-glass spectra due to oxygen doping in cobaltates

W. Peng[1,7], H. Guo[1,2], W. Schmidt[3], A. Piovano[4], H. Luetkens[5], C.-T. Chen[6], Z. Hu[1] & A. C. Komarek[1]

The magnetic excitation spectrum of most high-temperature superconducting (HTSC) cuprates is hour-glass shaped. The observation of hour-glass spectra in the isostructural Sr-doped cobaltates $La_{2-x}Sr_xCoO_4$ gives rise to a deeper understanding of these spectra. So far, hour-glass spectra have been only observed in those systems that evolve from incommensurate magnetic peaks. Here, we report on the appearance of hour-glass spectra in oxygen-doped cobaltates $La_2CoO_{4+\delta}$. The high-energy part of the hour-glass spectrum of oxygen doped cobaltates is extremely anisotropic with a very prominent stripe-like appearance not seen that clearly in purely Sr-doped compounds. A charge stripe scenario is evidenced by (polarized) neutron diffraction measurements and also corroborated by spin wave simulations. Our results indicate that charge stripes are the origin of the anisotropic stripe- or diamond-shaped high-energy part of the hour-glass spectrum. A link between hour-glass spectra and charge stripes could be of relevance for the physics in HTSC cuprates.

Many classes of high-temperature superconducting (HTSC) cuprate materials have been discovered since its initial discovery in 1986[1] but the underlying superconducting pairing mechanism remains enigmatic. A universal property of most HTSC copper oxides is the presence of so-called hour-glass magnetic spectra[2–12]. Also these spin excitation spectra have been discussed controversially in the past[13–16]. The observation of such kind of spectra in an isostructural copper-free reference system could be a key for the solution of the long-standing puzzle of the origin of these spectra. The observation of hour-glass spectra in cobaltates[17] was the first observation of these kind of spectra in an isostructural copper-free compound. Especially, the absence of metallic properties in these Co oxide materials could rule out one important scenario for hour-glass spectra based on Fermi surface effects[17]. An alternative scenario is based on charges segregating into stripes[18–24]. However, also the origin of hour-glass spectra in these cobaltates - initially assumed to be related to such charge stripe phases[17,25,26] - is still debated since alternative explanations came up which are based on nano phase separation of "$La_{1.5}Sr_{0.5}CoO_4$-like" checkerboard charge ordered (CBCO) and "La_2CoO_4-like" undoped regions[27,28]. Therein, no unambiguously visible or only weak (or unclear) signatures of charge stripes[27–33] could be detected in the Sr-doped cobaltate system (free from oxygen excess). So far, all observations made in this hole-doped Co oxide system have in common that the hour-glass spectrum arises from incommensurate magnetic peaks close to third-integer positions in reciprocal space i.e. at $\mathbf{Q} = \mathbf{Q_{AFM}} \pm (\epsilon, \pm\epsilon, 0)$ with $\mathbf{Q_{AFM}} = (H + 1/2, K + 1/2, L)$ being the wavevector of the unmodulated antiferromagnetic $\uparrow\downarrow\uparrow$ spin configuration.

Here, we report on the observation of hour-glass spectra in the oxygen-doped cobaltate $La_2CoO_{4.20}$ that do not arise from a clearly incommensurate magnetic phase as is observed in Sr-doped cobaltates. Instead a commensurate diagonal $\bullet\uparrow\bullet\downarrow\uparrow\bullet$ charge stripe phase with $\epsilon = 1/5$ appears in this system which already exists at high temperatures above room temperature (where already ~90% of the charge stripe ordering superstructure reflection intensity is attained). We conclude that it is this phase that is responsible for the striped shape of the high-energy part of the hourglass spectrum that is very evident in this oxygen-doped cobaltate.

Results and Discussion

Inelastic neutron scattering

The magnetic excitation spectrum of $La_2CoO_{4.20}$ is shown in Fig. 1. As expected for an hour-glass spectrum, the magnetic excitations disperse from the magnetic satellite positions inwards and merge around ~15 meV before dispersing outwards again. The magnetic nature of these excitations was ascertained with polarized neutron scattering measurements, see Fig. 1c. Moreover, polarization analysis also provides information about the nature of these excitations that are in-plane excitations, i.e., the entire oscillation of

[1]Max-Planck-Institute for Chemical Physics of Solids, Nöthnitzer Str. 40, D-01187 Dresden, Germany. [2]Songshan Lake Materials Laboratory, Dongguan, Guangdong 523808, China. [3]Forschungszentrum Jülich GmbH, Jülich Centre for Neutron Science at ILL, 71 avenue des Martyrs CS 20156, 38042 Grenoble, France. [4]Institut Laue-Langevin (ILL), 71 Avenue des Martyrs, 38042 Grenoble, France. [5]Laboratory for Muon Spin Spectroscopy, Paul Scherrer Institut, 5232 Villigen PSI, Switzerland. [6]National Synchrotron Radiation Research Center 101Hsin-Ann Road, Hsinchu, 30076, Taiwan. [7]Present address: Institute for Advanced Study, Shenzhen University, Shenzhen, 518051, China. e-mail: Komarek@cpfs.mpg.de

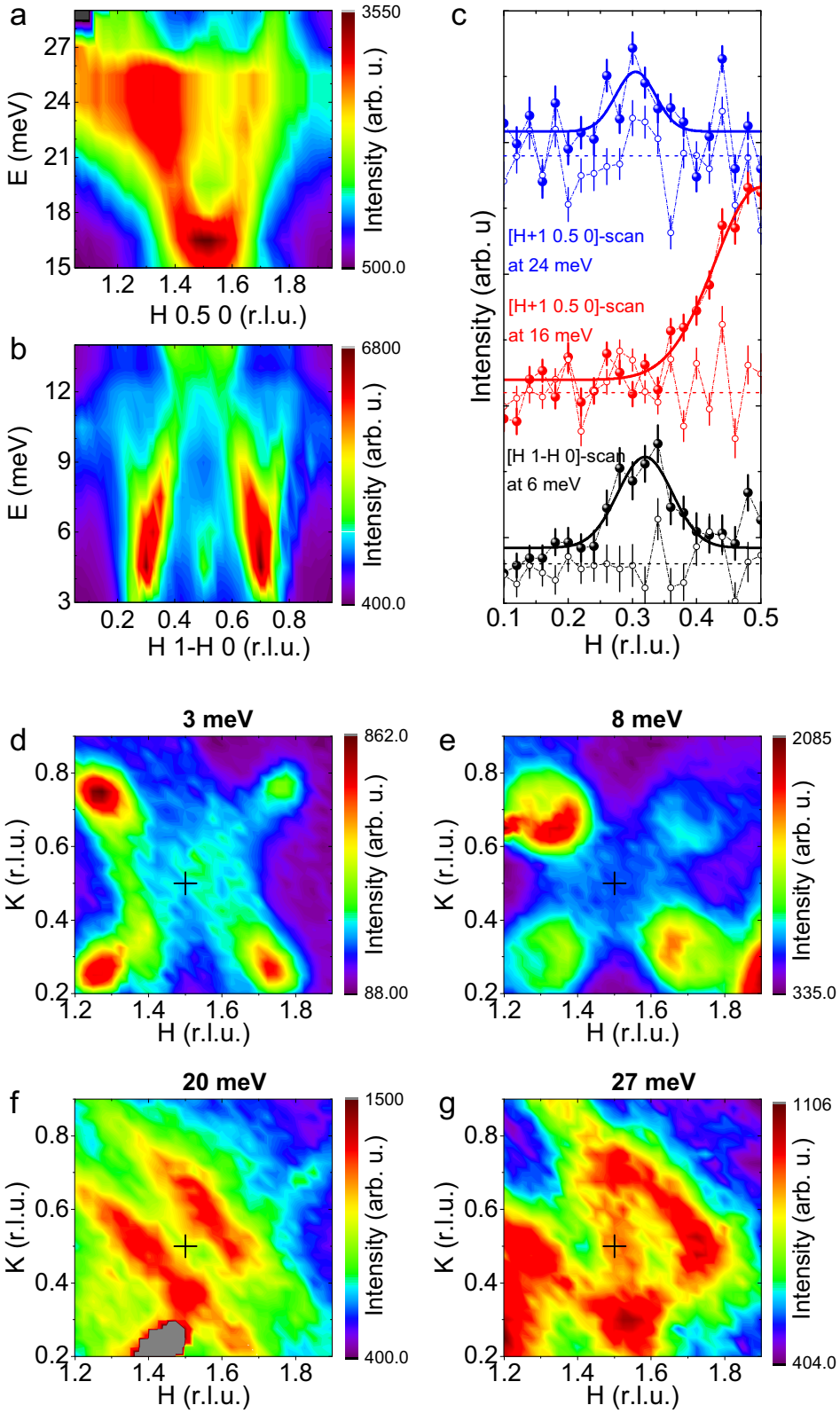

Fig. 1 | Appearance of an Hour-glass spectrum. All spectra were measured and normalized to a fixed monitor rate. **a** High and (**b**) low energy magnetic excitation spectra of $La_2CoO_{4.20}$. The magnetic exciatation spectrum of $La_2CoO_{4.20}$ has an hour-glass shape similar to that observed in the $La_{2-x}Sr_xCoO_4$-system[17,28,33]. **c** Longitudinal polarized inelastic neutron scattering measurements for $La_2CoO_{4.20}$ at 2 K; solid/open symbols: magnetic neutron scattering intensities for in-plane (M_y) and out-of-plane (M_z) excitations. (Note that the x-direction is parallel to **Q**, the $z-$direction is equal to the c-direction and y is perpendicular to both.) The intensities were corrected for imperfect flipping ratio R and normalized by the isotropic magnetic form factor $f(Q)$ of Co^{2+}, i.e., $M_y = \frac{R+1}{R-1}(\sigma_{x\bar{x}} - \sigma_{y\bar{y}})/f^2(Q)$ and $M_z = \frac{R+1}{R-1}(\sigma_{x\bar{x}} - \sigma_{z\bar{z}})/f^2(Q)$. For clarity the different constant-E scans were shifted as indicated by the dashed lines. The solid curves are the Gaussian fits to M_y intensities. The calculation of error bars is described in the Methods section. **d**–**g** Additional constant-E slices showing the hour-glass shape of magnetic excitations. **f**, **g** At higher energies the spectrum becomes extremely anisotropic with the magnetic neutron scattering intensities being distributed over four distinct bands ("stripes") arranged diagonally around $\mathbf{Q_{AFM}}$. (**g**) These "stripes" are responsible for the diamond-shape of the high-energy spectrum.

the spins is confined to the cobalt oxygen planes. Constant energy slices are shown in Fig. 1d–g. Interestingly the high-energy part is extremely anisotropic in oxygen doped cobaltates and the excitations have a stripe-like appearance with four crossing lines centered around $\mathbf{Q_{AFM}}$. This is in contrast to the much more isotropic high-energy spectra in Sr-doped cobaltates (without larger oxygen excess δ)[27,28]. Such stripe-shaped high-energy excitations could either point to the presence of diagonal charge stripes or to the presence of one strong diagonal exchange interaction J^{diag} in a single diagonal direction (either [1 -1 0] or [1 1 0]) for an alternative scenario without charge stripes.

Elastic neutron scattering

Further insight into the spin configurations could be obtained by polarized elastic neutron scattering measurements, see Fig. 2a, b. Also here, magnetic and structural contributions can be distinguished by polarization analysis. The structural contribution that can be observed at half-integer positions in reciprocal space could be related to charge ordering or to octahedral tilts. Other structural contributions also arise from oxygen ordering. In addition to these expected structural contributions there appear magnetic intensities at low temperatures, see Fig. 2c, e. There are different kind of commensurate magnetic reflections at peak positions with ϵ = 0, 1/4 and 1/5. First of all, magnetic intensities can be found at $H \sim 0.3$ and 0.7 (ϵ = 1/5) for this oxygen doped compound, see Fig. 2e. The additional observation of the corresponding charge stripe peaks – see Fig. 3a – indicates that these magnetic reflections are related to a charge stripe phase. Here we will call this stripe phase "composite" charge stripe phase, see Fig. 3d–f. This is also corroborated by our spin wave simulations, see Fig. 4a. At first glance, the magnetic reflection that is centered at half-integer positions in reciprocal space (ϵ = 0) might indicate Co^{2+}-Co^{2+} nearest-neigbouring antiferromagnetic (nn-AFM) correlations (J) that can be also observed in undoped La_2CoO_4[27,34] and lower-Sr-doped $La_{2-x}Sr_xCoO_4$ (for Sr-doping levels below roughly 33%)[27,33]. However, our simulations – see Fig. 4a – provide evidence that even this half-integer magnetic reflection originates from the same commensurate charge stripe phase – the "composite" charge stripe phase shown in Fig. 3f. The identical temperature dependence for both kind of magnetic signals (with ϵ = 1/5 and 0) that can be seen in Fig. 2e, f supports this latter scenario. The next set of magnetic reflections that can be found at quarter-integer positions (ϵ = 1/4) – see Fig. 2c (*blue data points*) – might indicate Co^{2+}-Co^{3+}-Co^{2+} next-nearest-neigbouring antiferromagnetic (nnn-AFM) correlations (J') with straight exchange paths as observed in half-doped ($Co^{2.5+}$) checkerboard charge ordered $La_{1.5}Sr_{0.5}CoO_4$[35] and could be the result of disorder or inhomogeneities that lead to CBCO regions in parts of the sample (phase separation).

This observation of commensurate magnetic peaks is very different from the case of the $La_{2-x}Sr_xCoO_4$ system where only one set of clearly incommensurate magnetic reflections appears at positions in reciprocal space that are between these sets of commensurate magnetic reflections - see the *magenta data points* for a Sr-doped reference sample[33] in Fig. 2c. Polarized neutrons help to understand this difference: Instead of the known easy-plane anisotropy (*ab* plane) for the Sr-doped cobaltates[28] we observe a unidirectional easy axis anisotropy for this oxygen doped cobaltate. This is evidenced by the absence of any detectable intensities for magnetic moments in direction of the propagation vector in polarized neutron measurements - see Fig. 2c. For the phase with magnetic peaks at ($\delta\delta$ 7) the magnetic moments orient basically only in transversal directions since $\sigma^{corr.}_{\bar{x}x} - \sigma^{corr.}_{zz}$ is non-zero and since $\sigma^{corr.}_{\bar{x}x} - \sigma^{corr.}_{\bar{y}y}$ is essentially zero, i.e., $M_z > 0$, $M_y = 0$. (Note that the z-direction is the crystallographic [1 $\bar{1}$ 0]-direction in tetragonal notation, the x-(y-)direction is roughly the $[0\,0\,1]_{tet}$-direction ($[1\,1\,0]_{tet}$-direction) for small values of δ. Also for the ϵ = 1/5 magnetic phase the spins are transversally aligned.) This unidirectional anisotropy is probably the consequence of the distorted crystal structure of these oxygen doped cobaltates with an elongation of the unit cell in one of the diagonal directions[36] (in addition to the elongation in out-of-plane

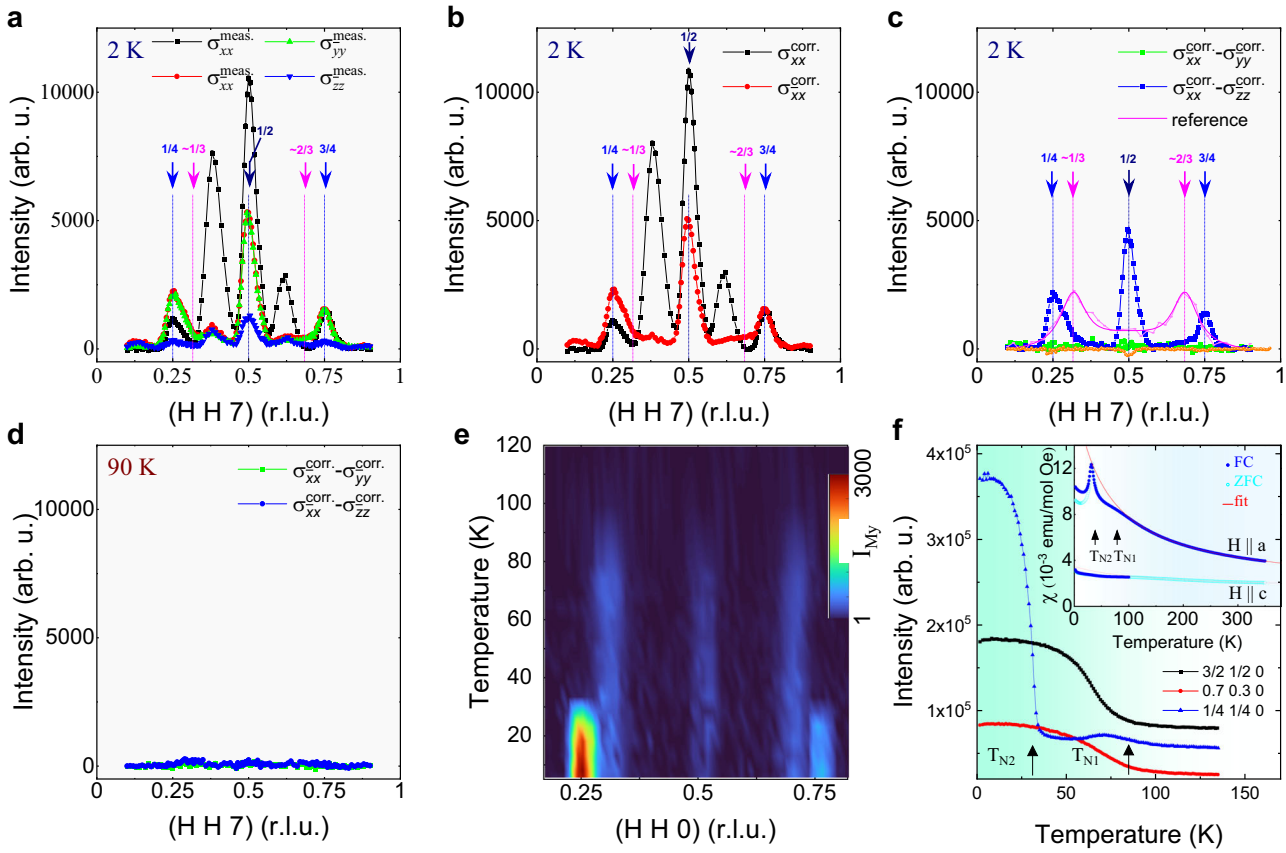

Fig. 2 | Magnetic correlations. a–d Longitudinal polarized neutron scattering measurements. 2 K and 90 K measurements are compared for different polarization channels. (Here, the x-/y-axes are defined along the direction parallel/perpendicular to **Q** both being within the scattering plane, and the z-axis is perpendicular to the scattering plane.) In the spin-flip (SF)/non-spin-flip (NSF) channels $\sigma_{\bar{x}x}$ / σ_{xx} only magnetic/nonmagnetic contributions are detected. By the comparison of the three SF channels a collinear magnetic moment direction is revealed in figure (**c**). For comparison, also the magnetic intensities of a $La_{1.63}Sr_{0.37}CoO_4$ reference sample are shown (*magenta data points*); taken from a $H\bar{H}0$-scan[33]). The intensity scales are the same in figures (**a**–**d**). **e** The temperature and **Q**-dependence of the magnetic peak intensities is shown for polarized neutrons with $I_{M_y} = \sigma^{corr.}_{x\bar{x}} - \sigma^{corr.}_{\bar{y}y}$. **f** A complementary measurement of the detailed T-dependence at certain **Q**-points with unpolarized neutrons. The inset shows the magnetic susceptibility χ(T) of $La_2CoO_{4.20}$. The calculation of error bars is described in the Methods section.

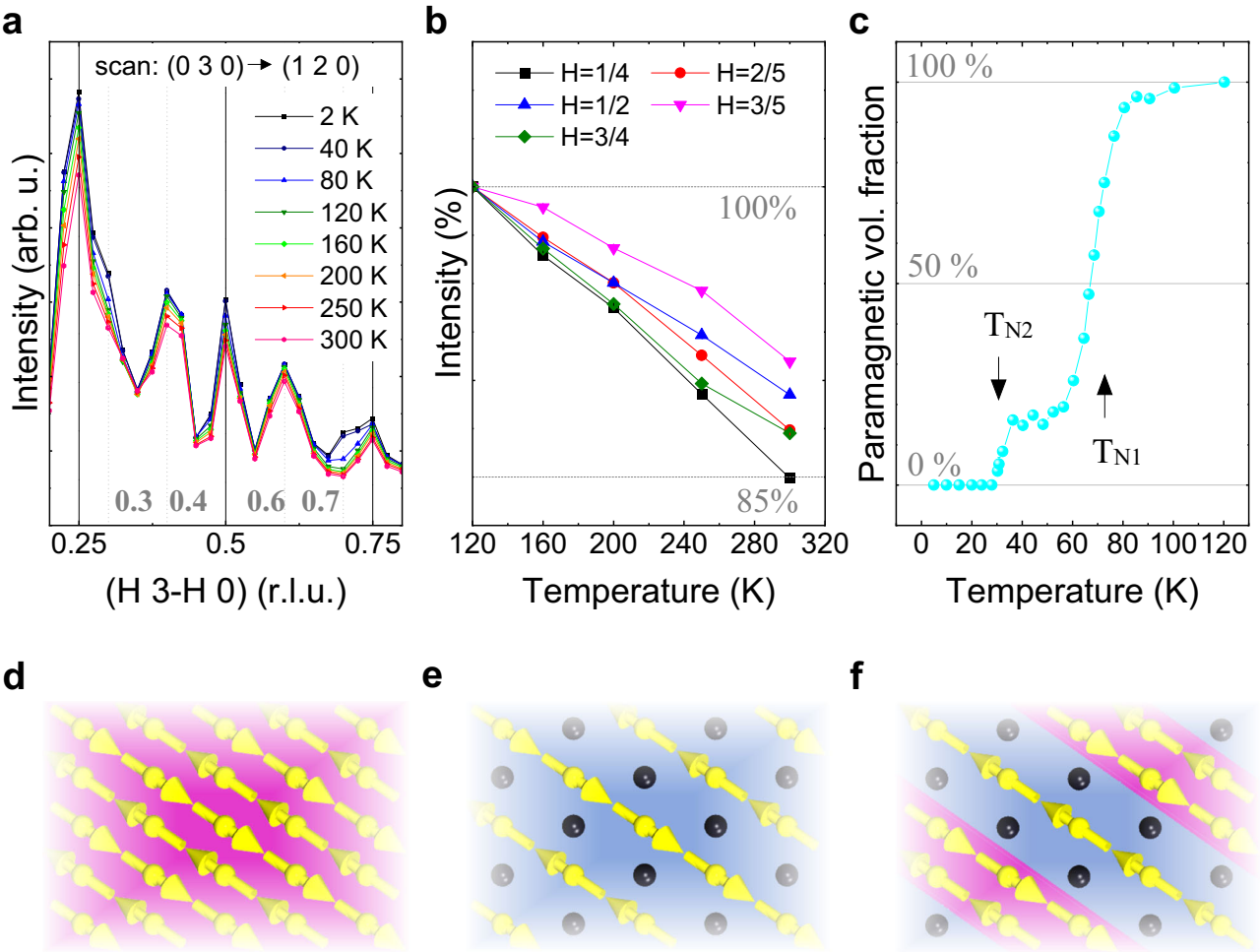

Fig. 3 | Charge correlations and μSR data. a Neutron scans for diagonal scans through (0.5 2.5 0) at different temperatures which are showing magnetic and structural peak intensities. For a charge stripe phase with a magnetic peak at H = 0.3, 0.7 one would expect a structural charge ordering peak at H = 0.4, 0.6. The latter peaks appear already almost fully developed at room temperature with a temperature dependence very similar to that of all other structural features like oxygen ordering or octahedral tilting reflections etc. (→ Debye Waller factor). Due to the high statistics the error bars are smaller than the symbol size. The calculation of error bars is described in the Methods section. **b** Also the temperature dependence shows that the charge stripe phase is already (almost) fully developed at room temperature. **c** The paramagnetic volume fraction as detected in μSR experiments. Similar as for χ(T) only two transitions can be resolved. Importantly, these measurements show that the charge stripe phase is the dominating 84% majority phase in this oxygen doped cobaltate. The calculation of error bars is described in the Methods section. **d–f** Schematic models for three possibly occuring phases: (**d**) undoped, (**e**) checkerboard charge ordered and (**f**) "composite" charge stripe phase; yellow arrows: spins of Co^{2+}-ions, black spheres: non-magnetic Co^{3+}-ions.

direction that is also present in the tetragonal Sr-doped cobaltates). Due to the restriction to collinear spin structures within each structural domain in $La_2CoO_{4.20}$ first of all nn-AFM collinear ↑↓ spin arrangements (coupled with at least one *J*) or nnn-AFM collinear ↑•↓ spin arrangements (coupled only with weaker *J′*) are favored, see Fig. 3d, e. This would explain the observation of commensurate magnetism in $La_2CoO_{4.20}$ since a spiralling of the spins is hampered. Also the alternation of these two different spin arrangements in a regular manner would give stable collinear spin structures: charge stripes - see Fig. 3f. Hence, the appearance of a $\epsilon = 1/5$ magnetic phase could be naturally explained by charge stripe •↑•↓↑• spin arrangements that basically include a regular concatenation of the spin arrangements with $\epsilon = 0$ and $\epsilon = 1/4$ in an alternating manner (since the charges should be centered at the Co sites in these highly insulating and rather ionic cobaltates) - see Fig. 3f. A periodic alternation of charge ordered domains of this kind would be also consistent with the value of $\epsilon = 1/5$.

The corresponding charge stripe ordering superstructure reflections could be expected to appear in diagonal scans at $H = (0+2\epsilon)$ and $(1-2\epsilon)$[22]. Therefore, we studied the temperature dependence of the reflections observed in these diagonal scans at H =0.4, 0.6, see Fig. 3a, b. These charge stripe ordering superstructure reflections are present already at room temperature and their temperature dependence does not show any indication for a structural phase transition between room-temperature and the onset of magnetic ordering as would be expected usually for a charge stripe phase[32]. Instead, the temperature dependence of these reflections is small and quite linear without any indication for a transition (jump etc.) and very similar to that of the other purely structural reflections with of the order of 90% of their intensity already attaining at room temperature. Hence, these reflections do not belong to a phase that is emerging below room-temperature as expected usually for a charge stripe phase[32]. Our detected charge stripe phase would set in distinctly above room-temperature. But this is exactly what is also observed for checkerboard charge ordering in these cobaltates[33]. The emergence of these superstructure reflections is also a difference to the Sr-doped cobaltates where these reflections could not be observed for the same kind of scans in a Sr-doped sample (without larger oxygen excess) which has nominally the same hole-doping level of ~ 40%[27].

Spin wave simulations

Finally, we made spin wave simulations for such a "composite" charge stripe phase shown in Fig. 3f. A detailed description of our model can be found in the Methods section and a further discussion is also presented in

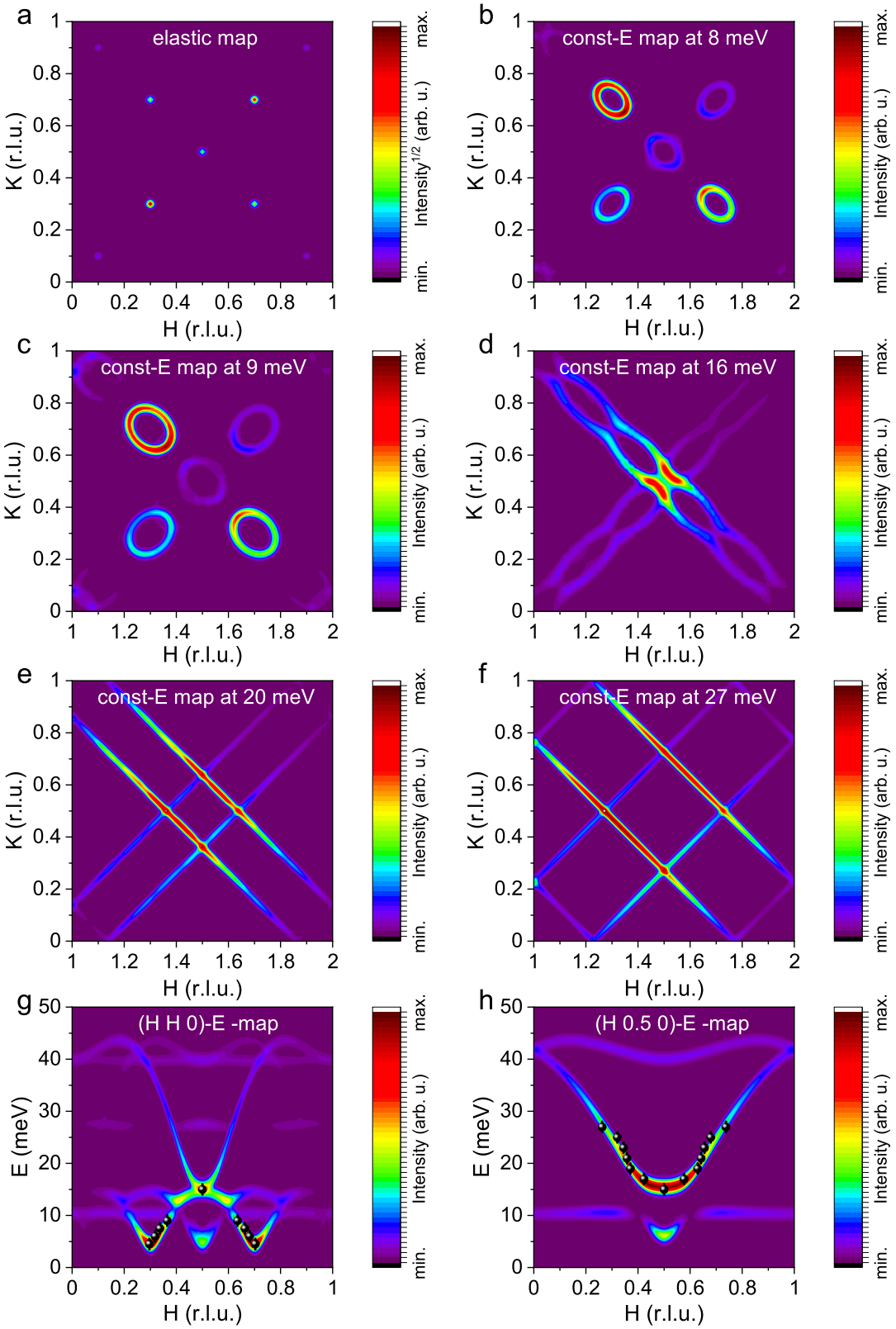

the Supplementary Mat. file. First of all the elastic map shown in Fig. 4a reproduces magnetic peaks at the experimentally observed magnetic peak positions. The strongest magnetic peaks in these simulations can be found at (0.3, 0.3), (0.3, 0.7), (0.7, 0.3) etc. within the *HK* plane of reciprocal space. This corresponds to magnetic peaks of the ϵ = 1/5 phase. Furthermore, these simulations show that also the ϵ = 0 magnetic signal at (1/2, 1/2) that simultaneously appears together with the aforementioned ϵ = 1/5 magnetic peaks at T_{N1} belong to the same phase – the "composite" charge stripe phase – which is in agreement with our magnetic susceptibility and μSR measurements. Our μSR data shown in Fig. 3c confirms that this charge stripe phase is the 84% majority phase in this material. (The small contributions of the remaining minority phase

Fig. 4 | Spin wave simulations. The results of our simulations with *McPhase* for a "composite" charge stripe phase are shown. **a** First of all the elastic neutron scattering intensities within the *HK*0 plane are shown. For better visibility of weaker intensities, the square root of the intensities is shown in this elastic map. Also our simulations yield magnetic peaks at (0.3 0.7 0) and (0.7 0.3 0) etc. Furthermore, a weaker magnetic peak at (0.5 0.5 0) can be observed as well. This shows that the experimentally observed half-integer magnetic peaks do not belong to yet another phase but that such additional peaks occur in a "composite" charge stripe phase. **b**–**f** Calculated constant energy slices of the simulated spin excitation spectrum. In panels (**b**) and (**c**) it can be seen how spin wave cones evolve from the magnetic peak positions. In panel (**d**) the origin (emergence) of the stripe-like high-energy spectrum at energies directly above the neck of the hour-glass spectrum (at 15.5 meV) is shown. Panels (**e**, **f**) show how the stripe-like (diamond-shaped) high-energy spectrum develops at higher energies. **g**, **h** The calculated dispersion in energy-momentum space for diagonal *HH*0-scans and vertical/horizontal *H*0.5 0-scans is shown. Experimentally obtained data is plotted with black dots on top of the spectra. The calculation of error bars is described in the Methods section. Note that the outwards-dispersing (low-energy) branches will be suppressed by disorder occuring in "real" charge stripe systems[50] and any imperfections in the "real" material will also broaden the spectra.

that is associated with the magnetic signal at quarter-integer positions below T_{N2} will be barely visible in inelastic neutron measurements and can be neglected – especially at somewhat higher energies where the spectra of half-doped cobaltates show no magn. dispersions[35]).

Our spin wave simulations are able to reproduce all essential parts and features of the experimentally observed hour-glass magnetic spectrum as can be seen from a comparison of Figs. 1 and 4 or in the direct comparison presented in Supplementary Figs. S7 & S8. As can be seen, the occurrence of a "composite" charge stripe phase is able to explain the strongly anisotropic, (diamond) stripe-shaped excitation spectrum at higher energies that directly starts to develop above the neck of the hour glass spectrum - see Fig. 4d.

We would also like to note that two inequivalent Co^{2+} sites – indicated by the blue and red shaded areas in Fig. 3f – appear in this "composite" charge stripe phase which have different ionic environments. This is a difference to the case of the undoped parent material or to an ideal 1/3-doped charge stripe phase or also to an ideal half-doped CBCO phase where all Co^{2+} sites have an equivalent oxygen environment. For the "composite" charge stripe phase, we were not able to simulate the hour-glass spectrum properly if we used the same crystal field parameters for both inequivalent Co^{2+} sites ("CBCO" and "undoped" sites) – see the Supplementary Mat. file. (Note that such two inequivalent sites also appear in a nano phase separation scenario in Sr-doped cobaltates[28]). Also for the "composite" charge stripe model the high-energy excitations are related to excitations within the stripes and along the stripe direction between the "undoped" sites coupled with large exchange interactions *J*, see the Supplementary Fig. S13 and the Supplementary Movie 1. This resembles a nano phase separation scenario[28], where the high-energy excitations were also attributed to the same type of "undoped" regions, but where these regions need not be stripe-shaped.

Conclusion

A main difference between oxygen and Sr-doped cobaltate systems is the collinear spin arrangement due to an easy axis anisotropy in the oxygen doped material with a crystal structure that hampers a spiralling of the spins within the Co oxygen planes and, thus, supports the development of commensurate magnetism (Fig. 3d–f) as is indicated by the re-distribution of magnetic intensities away from a single set of clearly incommensurate magnetic peak positions (as observed for Sr-doped cobaltates[28]) to commensurate peak positions. The difference between oxygen- and Sr- doped cobaltates highlights also the role of structural distortions and oxygen content for the emergence of charge stripes.

Importantly, these unique observations reveal a connection between anisotropic high-energy spectra and the presence of charge stripe phases which is revealed by the comparison of oxygen-doped and Sr-doped cobaltates (without oxygen excess). In contrast to purely Sr-doped cobaltates[27–31,33] charge stripes play the dominant role in this oxygen doped cobaltate which, in turn, exhibits extremely anisotropic high-energy spectra with a very well pronounced diamond or stripe-like shape. This part of the spectrum is more isotropic[27,28] for Sr-doped cobaltates where also structural signatures of charge stripes are either absent[27] or barely visible (small)[33]. Especially, in the isovalent Sr-doped compound $La_{1.6}Sr_{0.4}CoO_4$ there is no evidence of similar reflections of the charge stripe order as in $La_2CoO_{4.20}$ and at high energies the spectrum of $La_{1.6}Sr_{0.4}CoO_4$ shows no stripe-like appearance[27]. Hence, the different observations in $La_2CoO_{4.20}$ and $La_{1.6}Sr_{0.4}CoO_4$ could have direct relevance for an understanding of the HTSC cuprates where fluctuating charge stripes are believed to be relevant to the superconducting pairing mechanism[37–39]. e.g., Ba-doped La_2CuO_4 (LBCO) materials are also governed by charge stripes and also exhibit rather anisotropic high-energy spin excitation spectra[2]. But for other cuprates like the Sr-doped counterparts $La_{2-x}Sr_xCuO_4$ (LSCO) quite isotropic high-energy spectra have been observed[8,40]. Since even slowly fluctuating charge stripes would be expected to produce a similar magnetic response as static ones, our findings might suggest that the shape of the high-energy part of the hourglass spectrum could probably be taken as a fingerprint for the absence or presence of a significant role of charge stripes for these spectra.

Methods

Crystal synthesis

$La_2CoO_{4+\delta}$ single crystals have been grown by the optical floating zone technique using a CSC four-mirror image furnace following the procedures in ref. 27. Powder X-ray diffraction measurements have been performed on a *Bruker D8 Discover A25* powder X-ray diffractometer, see Supplementary Fig. S1. These measurements indicate that $La_2CoO_{4.20}$ is impurity-free. All observable peaks can be described (Rietveld refinement) with an (average) orthorhombic structure model with space group *Bmeb* as was done for $La_2CoO_{4.22}$[41]. (Note that the true symmetry is incommensurate - probably with superspace group $F2/m(\alpha\beta0)0s$[36]). The lattice constants amount to a = 5.5268(10) Å, b = 5.4806(10) Å and c = 12.5870(28) Å. The crystals are single crystals as ascertained by Laue X-ray and neutron diffraction techniques, see Supplementary Fig. S1. Due to the lower than tetragonal symmetry, these single crystals are twinned. The excess oxygen content δ has been determined by thermogravimetric measurements on 80.03 mg sample mass to be $\delta = 0.20$. Single crystal X-ray diffraction measurements have been performed on a *Bruker D8 VENTURE* single-crystal X-ray diffractometer equiped with a Photon large area CMOS detector. The X-ray diffraction pattern are similar as the ones for $La_2CoO_{4.19}$ in ref. 36.

μSR measurements

Zero-field (ZF) and weak transverse field (wTF) muon spin relaxation (μSR) measurements have been performed on the GPS instrument at PSI, Switzerland, see Supplementary Fig. S2. Nearly 100% spin polarized muons were injected into the sample, and the decayed positrons which were ejected preferentially along the muon spin direction are accumulated by the forward and backward counters. The asymmetry is defined as $A(t) = [N_F(t) - \alpha N_B(t)]/[N_F(t) + \alpha N_B(t)]$, where $N_F(t)$ ($N_B(t)$) is the number of positrons that arrived at the forward (backward) counter at time t, and the parameter α reflects the different counting efficiencies of the counters. The muon events are counted in the veto mode, resulting in nearly zero background. The data were analyzed using the *Musrfit* package.

For a determination of the paramagnetic volume fraction of the sample wTF μSR spectra have been also measured in an external transverse field of 30 G (which results in a heavily damped signal for magnetically ordered phases and an oscillating signal for paramagnetic phases). The amplitude of the oscillating signal A_{PM} has been extracted from a fit of $A(t) = A_{PM} \cdot \cos(\gamma_\mu B_{ext} t + \varphi) \exp(-\lambda_{PM} t) + A_{tail} \cdot \exp(-\lambda_{tail} t)$ to the spectra. The temperature dependence of the paramagnetic volume fraction is proportional to A_{PM}. The error bars are the standard errors of the fit using the

Musrfit package. Below 30 K, the parameters and the error bars are zero since no oscillation is detectable.

X-ray absorption spectroscopy (XAS) measurements

XAS spectra of $La_2CoO_{4.20}$ were measured using a bulk sensitive fluorescence yield method for the O - K edge and total electron yield for the Co $L_{2,3}$ edge at the TLS11A beamline of the National Synchrotron Radiation Research Center (NSRRC) in Taiwan, see Supplementary Fig. S3. For energy calibration NiO and CoO single crystals were measured simultaneously for the O - K edge and the Co - L edge spectra, respectively. First of all these XAS measuremenets confirm an average Co valence state of +2.40(2) in our single crystals, i.e., that the composition is $La_2CoO_{4.20(1)}$ with 40% Co^{3+} ions in this material. These Co^{3+} ions could be either in the low spin (LS), intermediate spin (IS) or high spin (HS) state[42]. Our XAS measurements show that the Co^{3+} ions in $La_2CoO_{4.20}$ are in a non-magnetic low spin (S=0) state. Further details can be found in the Supplementary Mat. file.

Neutron scattering measurements

Unpolarized elastic and inelastic neutron scattering measurements have been performed on the IN8 spectrometer at Institut Laue-Langevin (ILL) in Grenoble, France. Doubly focused Si(111) monochromator and pyrolytic graphite (PG) analyzer were used with a PG filter mounted behind the sample. The final neutron wave vector was fixed to 2.662 $Å^{-1}$. In Supplementary Fig. S4 selected neutron scans together with Gaussian fits are shown. Elastic neutron scattering measurements with longitudinal polarization analysis were performed on the IN12 spectrometer equipped with doubly focused PG monochromator and Heusler analyzer (k = 2.5 $Å^{-1}$). A velocity selector was used for suppression of higher order contaminations. The flipping ratio amounts to ~ 19.0. In Fig. 2b, c, the neutron scattering intensities have been corrected for imperfect neutron polarization (flipping ratio R) and background (bg) as follows: $\sigma_{\bar{x}x}^{\mathrm{corr.}} = R/(R-1)\cdot(\sigma_{\bar{x}x} - bg) - 1/(R-1)\cdot(\sigma_{xx} - bg)$, $\sigma_{xx}^{\mathrm{corr.}} = R/(R-1)\cdot(\sigma_{xx} - bg) - 1/(R-1)\cdot(\sigma_{\bar{x}x} - bg)$; and in Fig. 2e the data was corrected as follows: $(\sigma_{\bar{x}x}^{\mathrm{corr.}} - \sigma_{\bar{y}y}^{\mathrm{corr.}}) = ((\sigma_{\bar{x}x} - bg) - (\sigma_{\bar{y}y} - bg))\cdot(R+1)/(R-1)$, $(\sigma_{\bar{x}x}^{\mathrm{corr.}} - \sigma_{\bar{z}z}^{\mathrm{corr.}}) = ((\sigma_{\bar{x}x} - bg) - (\sigma_{\bar{z}z} - bg))\cdot(R+1)/(R-1)$; figures (a–f) have the same intensity scale. Complementary elastic neutron scattering measurements with longitudinal polarization analysis were performed on the IN22 spectrometer equipped with vertically focusing monochromator PG (002) and Heusler (111) analyzer (k = 2.662 $Å^{-1}$; flipping ratio: ~ 13.6; $I_{M_y} = \sigma_{x\bar{x}}^{\mathrm{corr.}} - \sigma_{y\bar{y}}^{\mathrm{corr.}}$). A velocity selector was used for suppression of higher order contaminations. Polarized inelastic neutron scattering measurements have been performed on the IN20 spectrometer (equipped with a cryopad polarimeter, double focusing Heusler (111) monochromator and analyzer with k_f = 2.662 $Å^{-1}$). The flipping ratio R amounts to ~ 19.6. Herein, we always refer to the *I4/mmm* unit cell setting ($a = b \sim 3.89$ Å and $c \sim 12.55$ Å; $a_{\mathrm{ortho}}, b_{\mathrm{ortho}} \sim \sqrt{2}\cdot a_{\mathrm{tet}}$). Error bars in presentations of experimental neutron scattering data are typically calculated by the square root of intensities. In Fig. 1c the intensities I and error bars δI were calculated as follows: $I_{M_y} = \sigma_{x\bar{x}}^{\mathrm{corr.}} - \sigma_{y\bar{y}}^{\mathrm{corr.}}$, $\delta I_{M_y} = \sqrt{(\delta\sigma_{x\bar{x}}^{\mathrm{corr.}})^2 + (\delta\sigma_{y\bar{y}}^{\mathrm{corr.}})^2}$ with $\delta\sigma_{x\bar{x}}^{\mathrm{corr.}} = \sqrt{\sigma_{x\bar{x}}^{\mathrm{corr.}}}$ and $\delta\sigma_{y\bar{y}}^{\mathrm{corr.}} = \sqrt{\sigma_{y\bar{y}}^{\mathrm{corr.}}}$. In Fig. 3a, b the statistics is that high that the error bars calculated by the square root of intensities are of the symbol size or smaller. For each figure, listed below are the instruments used to collect the data shown in this figure: Fig. 1a, b: IN8, Fig. 1c: IN20, Fig. 1d–f: IN8, Fig. 2a–d: IN12, Fig. 2e, f: IN22 & Fig. 3a, b: IN22.

Calculations

We performed spin wave simulations using the *McPhase* program code[43]. Therefore, we employed a "composite" charge stripe model and averaged the resulting spectra for two different stripe domains as shown in Supplementary Fig. S5. For these calculations we first of all considered a strong AFM nearest neighbour isotropic Heisenberg exchange interaction (J) between the S = 3/2 spins and also a much weaker AFM exchange coupling J' across the holes (third-nearest neighbours) of the Co^{2+} ions. Note that these two exchange interactions were identified as the significant exchange interactions in Sr-doped cobaltates[28] and that our XAS measurements confirm that the Co^{3+} ions are in a nonmagnetic low spin state. Furthermore, we also considered spin orbit coupling ($\lambda\mathbf{L}\cdot\mathbf{S}$) and the impact of the single ion crystal fields on the Co^{2+} ions (L = 3, S = 3/2). This can be described by the following Hamiltonian:

$$\mathcal{H} = -1/2\sum_{i,j\in 1st} J\mathbf{S}_i\cdot\mathbf{S}_j - 1/2\sum_{i,j\in 3rd} J'\mathbf{S}_i\cdot\mathbf{S}_j + \sum_j\left[\sum_{l,m} B_l^m O_l^m(\mathbf{L}_j) + \lambda\mathbf{L}_j\cdot\mathbf{S}_j\right] \quad (1)$$

with crystal field parameters B_l^m and Stevens operator-equivalents O_l^m as well as the spin-orbit coupling parameter λ[35]. The first (second) sum in Eq. (1) considers nearest (3rd nearest) neighbour interactions only, see Supplementary Fig. S5. In refs. 17,34,35 this approach was described for these 2-1-4 cobaltates (e.g. for $La_{1.5}Sr_{0.5}CoO_4$). We started our simulations for $La_2CoO_{4.20}$ with the parameter values of $La_{1.5}Sr_{0.5}CoO_4$[35] for both of the two inequivalent Co^{2+} sites in our "composite" charge stripe model and with an additional parameter B_2^{-2} to properly account for the in-plane anisotropies, compare the Supplementary Mat. file. Note that this parameter is allowed for lower, monoclinic symmetries as can be expected for this oxygen doped cobaltate. (Even for Sr-doped cobaltates[28] we could imagine locally lower symmetries than generally assumed.) However, when using the same parameters for both inequivalent Co sites we were unable to describe the spectra with the initial starting parameters taken from ref. 35 or for variations of these parameters since low and high energy excitations were always separated by an energy gap then, see Supplementary Fig. S6. In order to close that energy gap between high and low energy excitations without losing the correct dispersion above the neck of the hour-glass it turned out to be beneficial to use different crystal field parameters B_l^m for the two inequivalent Co^{2+} sites, which we called "undoped" sites and "CBCO" sites, corresponding to the red shaded and blue shaded regions in Fig. 3f. The resulting simulated spectra are shown in Fig. 4. A direct comparison between simulation and experiment can be seen in Supplementary Figs. S7 & S8. The parameters that we used for these simulations (and that were obtained by iteratively adjusting their values until a reasonably good description of the experimental data was achieved) are listed in Supplementary Tab. S1. (The corresponding single ion energy levels are shown in Supplementary Fig. S9). Note that the crystal field parameters cannot be determined uniquely here – for further information see the Supplementary Mat. file.

We have chosen to present constant energy slices in Fig. 4b–f around (1.5, 0.5) instead of (0.5, 0.5) in order to allow for a direct comparison with the experiment: all features including even the experimentally observed asymmetry for the contributions of the two different stripe domains are also visible in our simulated spectra around (1.5, 0.5).

In Fig. 4 the "thickness" of the energy slices in energy space amounts to 1 meV (i.e., $\Delta E = \pm 0.5$ meV) for all constant energy maps, i.e., for panels (b–f). The experimentally observed spectra appear to be broader which might be the result of disorder in the real material. The spectra in energy-momentum space shown in panels (g–h) were folded with a Gaussian function with 2 meV FWHM to account for instrumental energy resolution and to some extent also for sample-intrinsic broadening of the spectrum. In Fig. 4g, h experimentally obtained data points (see the Supplementary Mat. file for further details) are plotted on top of the spectra in energy-momentum space. (The vertical error bars amount to 1 meV since the calculated pure instrumental energy resolution is already somewhat larger than 1 meV).

A detailed visualization of the simulated spectrum using constant-energy slices in steps of 1 meV is shown in Supplementary Fig. S10. And the

character of different types of excitations can be seen in the Supplementary Movie 1.

Finally, note that these hour-glass spectra can be also described with a much simpler approach (based on the "composite" charge stripe model) with a spin-only Hamiltonian with two single ion ansiotropy terms DS_z^2 and $E(S_x + S_y)^2$ only – see Supplementary Eq. (2) and Supplementary Figs. S11–S14 as well as Supplementary Tab S2 for the parameters used. In these simulations, the crystal field effects were treated in a simplified manner by only two parameters D and E, and the experimentally observed spectra can be described very well with this approach, see Supplementary Figs. S11 & S14.

Based on this simplified spin-only Hamiltonian further spin wave calculations using the *SpinW* program code can be found for $La_2CoO_{4.2}$ and related layered cobaltate systems $La_{2-x}Sr_xCoO_4$ (x = 0, 1/3, 1/2) in the Supplementary Mat. file, see Supplementary Figs. S15–S20 and Supplementary Tab. S3.

Data availability

Experimental data are available from the Institut Laue-Langevin (ILL)[44–49].

Code availability

Computer code is available from https://mcphase.github.io/webpage/ (*McPhase* version 5.5). The parameters used are listed in the Supplementary Materials file (Supplementary Tab. S1).

Received: 12 June 2023; Accepted: 3 December 2024;
Published online: 16 December 2024

References

1. Bednorz, J. G. & Müller, K. A. Possible high tc superconductivity in the Ba La Cu O system. *Z. Physik B* **64**, 189 (1986).
2. Tranquada, J. M. et al. Quantum magnetic excitations from stripes in copper oxide superconductors. *Nature* **429**, 534–538 (2004).
3. Matsuda, M. et al. Magnetic dispersion of the diagonal incommensurate phase in lightly doped $La_{2-x}Sr_xCuO_4$. *Phys. Rev. Lett.* **101**, 197001–197004 (2008).
4. Arai, M. et al. Incommensurate spin dynamics of underdoped superconductor $YBa_2Cu_3O_{6.7}$. *Phys. Rev. Lett.* **83**, 608–611 (1999).
5. Bourges, P. et al. The spin excitation spectrum in superconducting $YBa_2Cu_3O_{6.85}$. *Science* **288**, 1234–1237 (2000).
6. Christensen, N. B. et al. Dispersive excitations in the high-temperature superconductor $La_{2-x}Sr_xCuO_4$. *Phys. Rev. Lett.* **93**, 147002 (2004).
7. Hayden, S. M., Mook, H. A., Dai, P., Perring, T. G. & Dogan, F. The structure of the high-energy spin excitations in a high-transition-temperature superconductor. *Nature* **429**, 531–534 (2004).
8. Vignolle, B. et al. Two energy scales in the spin excitations of the high-temperature superconductor $La_{2-x}Sr_xCuO_4$. *Nature Phys.* **3**, 163–167 (2007).
9. Xu, G. et al. Testing the itinerancy of spin dynamics in superconducting $Bi_2Sr_2CaCu_2O_{8+\delta}$. *Nature Phys.* **5**, 642–646 (2009).
10. Lipscombe, O. J., Vignolle, B., Perring, T. G., Frost, C. D. & Hayden, S. M. Emergence of coherent magnetic excitations in the high temperature underdoped $La_{2-x}Sr_xCuO_4$ superconductor at low temperatures. *Phys. Rev. Lett.* **102**, 167002–167005 (2009).
11. Hinkov, V. et al. Spin dynamics in the pseudogap state of a high-temperature superconductor. *Nature Physics* **3**, 780–785 (2007).
12. Fujita, M. et al. Progress in neutron scattering studies of spin excitations in high- t c cuprates. *J. Phys. Soc. Jpn.* **81**, 011007–011025 (2012).
13. Eremin, I., Morr, D. K., Chubukov, A. V., Bennemann, K. H. & Norman, M. R. Novel neutron resonance mode in $d_{x^2-y^2}$-wave superconductors. *Phys. Rev. Lett.* **94**, 147001 (2005).
14. Vojta, M., Vojta, T. & Kaul, R. K. Spin excitations in fluctuating stripe phases of doped cuprate superconductors. *Phys. Rev. Lett.* **97**, 097001 (2006).
15. Seibold, G. & Lorenzana, J. Magnetic fluctuations of stripes in the high temperature cuprate superconductors. *Phys. Rev. Lett.* **94**, 107006 (2005).
16. Andersen, B. M., Graser, S. & Hirschfeld, P. J. Disorder-induced freezing of dynamical spin fluctuations in underdoped cuprate superconductors. *Phys. Rev. Lett.* **105**, 147002–147005 (2010).
17. Boothroyd, A. T., Babkevich, P., Prabhakaran, D. & Freeman, P. G. An hour-glass magnetic spectrum in an insulating, hole-doped antiferromagnet. *Nature* **471**, 341–344 (2011).
18. Zaanen, J. & Gunnarsson, O. Charged magnetic domain lines and the magnetism of high-T_c oxides. *Phys. Rev. B* **40**, 7391 (1989).
19. Schulz, H. J. Domain walls in a doped antiferromagnet. *J. Phys. (Paris)* **50**, 2833 (1989).
20. Machida, K. Magnetism in La_2CuO_4 based compounds. *Physica C* **158**, 192 (1989).
21. Tranquada, J. M., Sternlieb, B. J., Axe, J. D., Nakamura, Y. & Uchida, S. Evidence for stripe correlations of spins and holes in copper oxide superconductors. *Nature* **375**, 561 (1995).
22. Tranquada, J. M., Buttrey, D. J., Sachan, V. & Lorenzo, J. E. *Phys. Rev. Lett.* **73**, 1003 (1994).
23. Tranquada, J. M. et al. Simultaneous ordering of holes and spins in $La_2NiO_{4.125}$. *Phys. Rev. Lett.* **78**, 338 (1997).
24. Hücker, M. Structural aspects of materials with static stripe order. *Physica C: Superconductivity* **481**, 3–14 (2012).
25. Lancaster, T. et al. Stripe disorder and dynamics in the hole-doped antiferromagnetic insulator $La_{5/3}Sr_{1/3}CoO_4$. *Phys. Rev. B* **89**, 020405 (2014).
26. Williams, R. C. et al. Magnetic phase diagram of $La_{2-x}Sr_xCoO_4$ revised using muon-spin relaxation. *Phys. Rev. B* **93**, 140406(R) (2016).
27. Drees, Y., Lamago, D., Piovano, A. & Komarek, A. C. Hour-glass magnetic spectrum in a stripeless insulating transition metal oxide. *Nature Commun.* **4**, 2449 (2013).
28. Drees, Y. et al. Hour-glass magnetic excitations induced by nanoscopic phase separation in cobalt oxides. *Nat. Commun*. **5**, 5731 (2014).
29. Guo, H., Schmidt, W., Tjeng, L. H. & Komarek, A. C.Charge correlations in cobaltates $La_{2-x}Sr_xCoO_4$. *Phys. Status Solidii RRL* **9**, 580–582 (2015).
30. Li, Z. W. et al. Electronic and magnetic nano phase separation in cobaltates $La_{2-x}Sr_xCoO_4$. *J. Superconduct. Novel Magnet.* **29**, 727–731 (2016).
31. Li, Z. W. et al. Incommensurate spin correlations in highly oxidized cobaltates $La_{2-x}Sr_xCoO_4$. *Sci. Rep.* **6**, 25117 (2016).
32. Babkevich, P., Freeman, P. G., Enderle, M., Prabhakaran, D. & Boothroyd, A. T. Direct evidence for charge stripes in a layered cobalt oxide. *Nat. Commun.* **7**, 11632 (2016).
33. Guo, H. et al. Suppression of the outwards-dispersing branches in hour-glass magnetic spectra induced by nanoscale phase separation in $La_{2-x}Sr_xCoO_4$. *Phys. Rev. B* **100**, 014411 (2019).
34. Babkevich, P., Prabhakaran, D., Frost, C. D. & Boothroyd, A. T. Magnetic spectrum of the two-dimensional antiferromagnet La_2CoO_4 studied by inelastic neutron scattering. *Phys. Rev. B* **82**, 184425–184432 (2010).
35. Helme, L. M. et al. Magnetic order and dynamics of the charge-ordered antiferromagnet $La_{1.5}Sr_{0.5}CoO_4$. *Phys. Rev. B* **80**, 134414–134428 (2009).
36. Le Dréau, L.*Phase transitions and oxygen ordering in* $La_2CoO_{4+\delta}$ *and (T, T')-*La_2CuO_4*: single crystal growth and structural studies using synchrotron and neutron diffraction methods*. (Chemical Sciences. Université Rennes 1, 2011. English. NNT : 2011REN1S072.).
37. Kivelson, S. A., Fradkin, E. & Emery, V. J. Electronic liquid-crystal phases of a doped mott insulator. *Nature* **393**, 550–553 (1998).
38. Emery, V. J., Kivelson, S. A. & Zachar, O. Spin-gap proximity effect mechanism of high-temperature superconductivity. *Phys. Rev. B* **56**, 6120–6147 (1997).

39. Huang, E. W. et al. Numerical evidence of fluctuating stripes in the normal state of high-T_c cuprate superconductors. *Science* **358**, 1161–1164 (2017).
40. Matsuda, M., Granroth, G. E., Fujita, M., Yamada, K. & Tranquada, J. M. Energy-dependent crossover from anisotropic to isotropic magnetic dispersion in lightly doped $La_{1.96}Sr_{0.04}CuO_4$. *Phys. Rev. B* **87**, 054508–054512 (2013).
41. Aguadero, A., Alonso, J. A. & Daza, L. Oxygen excess in $La_2CoO_{4+\delta}$: A neutron diffraction study. *Z. Naturforsch.* **63b**, 615–622 (2008).
42. Kagan, M. Yu., Kugel, K. I. & Rakhmanov, A. L. Electronic phase separation: Recent progress in the old problem. *Phys. Rep.* **916**, 1–105 (2021).
43. Rotter, M., Duc Le, M., Bothroyd, A. T. & Blanco, J. A. Dynamical matrix diagonalization for the calculation of dispersive excitations. *J. Phys.: Condens. Matter* **24**, 213201–213220 (2012).
44. Komarek, A. C., Guo, H. & Piovano, A. Magnetic excitations in oxygen doped cobaltates. *Institut Laue-Langevin (ILL) doi:10.5291/ILL-DATA.4-02-491* (2018).
45. Komarek, A. C., Guo, H., Piovano, A. & ZHAO, L. Charge correlations and phase diagram of $La_2CoO_{4+\delta}$. Institut Laue-Langevin (ILL) https://doi.org/10.5291/ILL-DATA.5-15-614 (2017).
46. Komarek, A. C., Guo, H., Piovano, A. & Schmidt, W. First discovery of an hour-glass spectrum in oxygen doped cobaltates. Institut Laue-Langevin (ILL) https://doi.org/10.5291/ILL-DATA.4-02-540 (2018).
47. Komarek, A. C. et al. Different nanoscopic origin of upper and lower part of the hour-glass spectrum ? Institut Laue-Langevin (ILL) https://doi.org/10.5291/ILL-DATA.4-02-557 (2020).
48. Komarek, A. C., Peng, W. & Piovano, A. Hour-glass spectra from commensurate magnetic phases (i). Institut Laue-Langevin (ILL) https://doi.org/10.5291/ILL-DATA.4-02-595 (2020).
49. Komarek, A. C., Peng, W. & Schmidt, W. Hour glass spectrum without incommensurate magnetism. Institut Laue-Langevin (ILL) https://doi.org/10.5291/ILL-DATA.CRG-2699 (2020).
50. Andrade, E. C. & Vojta, M. Disorder, cluster spin glass, and hourglass spectra in striped magnetic insulators. *Phys. Rev. Lett.* **109**, 147201–147205 (2012).

Acknowledgements

The research in Dresden is supported by the Deutsche Forschungsgemeinschaft through Grant No. 320571839. We thank O. Stockert for helpful discussions. We thank M. Rotter for helpful discussions about McPhase simulations. We thank L. Zhao for assistance. We thank M. Schmidt and his team for thermogravimetric measurements. The work of H. G. was partially supported by the NSF of China (Grant No. 12004270) and the Guangdong Basic and Applied Basic Research Foundation (2019A1515110517). We acknowledge support from the Max Planck-POSTECH-Hsinchu Center for Complex Phase Materials.

Author contributions

Idea, project management: A.C.K.; single crystal growth: A.C.K.; neutron scattering measurements: W.P., H.G., W.S., and A.P.; μSR measurements: H.G. and H.L.; X.A.S. measurements: Z.H. and C.-T.C.; *SpinW* simulations: H.G.; *McPhase* simulations: A.C.K.; manuscript writing: A.C.K. with contributions from all other authors. W.P. and H.G. contributed equally.

Funding

Open Access funding enabled and organized by Projekt DEAL.

Competing interests

The authors declare no competing interests.

Additional information

Supplementary information The online version contains supplementary material available at https://doi.org/10.1038/s42005-024-01898-x.

Correspondence and requests for materials should be addressed to A. C. Komarek.

Peer review information *Communications Physics* thanks Clemens Ulrich and the other, anonymous, reviewer(s) for their contribution to the peer review of this work.